EUROPEAN ORGANIZATION FOR NUCLEAR RESEARCH

CERN–EP/2003-066

16 September 2003

Search for single top production via FCNC at LEP at $\sqrt{s}$=189-208 GeV

DELPHI Collaboration

Abstract

A search for single top production ($e^+e^- \rightarrow t\bar{c}$) via Flavour Changing Neutral Currents (FCNC) was performed using the data taken by the DELPHI detector at LEP2. The data analysed have been accumulated at centre-of-mass energies ranging from 189 to 208 GeV. Limits at 95% confidence level were obtained on the anomalous coupling parameters κ_γ and κ_Z.

(Accepted by Phys. Lett. B)

J.Abdallah[25], P.Abreu[22], W.Adam[51], P.Adzic[11], T.Albrecht[17], T.Alderweireld[2], R.Alemany-Fernandez[8], T.Allmendinger[17], P.P.Allport[23], U.Amaldi[29], N.Amapane[45], S.Amato[48], E.Anashkin[36], A.Andreazza[28], S.Andringa[22], N.Anjos[22], P.Antilogus[25], W-D.Apel[17], Y.Arnoud[14], S.Ask[26], B.Asman[44], J.E.Augustin[25], A.Augustinus[8], P.Baillon[8], A.Ballestrero[46], P.Bambade[20], R.Barbier[27], D.Bardin[16], G.Barker[17], A.Baroncelli[39], M.Battaglia[8], M.Baubillier[25], K-H.Becks[53], M.Begalli[6], A.Behrmann[53], E.Ben-Haim[20], N.Benekos[32], A.Benvenuti[5], C.Berat[14], M.Berggren[25], L.Berntzon[44], D.Bertrand[2], M.Besancon[40], N.Besson[40], D.Bloch[9], M.Blom[31], M.Bluj[52], M.Bonesini[29], M.Boonekamp[40], P.S.L.Booth[23], G.Borisov[21], O.Botner[49], B.Bouquet[20], T.J.V.Bowcock[23], I.Boyko[16], M.Bracko[43], R.Brenner[49], E.Brodet[35], P.Bruckman[18], J.M.Brunet[7], L.Bugge[33], P.Buschmann[53], M.Calvi[29], T.Camporesi[8], V.Canale[38], F.Carena[8], N.Castro[22], F.Cavallo[5], M.Chapkin[42], Ph.Charpentier[8], P.Checchia[36], R.Chierici[8], P.Chliapnikov[42], J.Chudoba[8], S.U.Chung[8], K.Cieslik[18], P.Collins[8], R.Contri[13], G.Cosme[20], F.Cossutti[47], M.J.Costa[50], B.Crawley[1], D.Crennell[37], J.Cuevas[34], J.D'Hondt[2], J.Dalmau[44], T.da Silva[48], W.Da Silva[25], G.Della Ricca[47], A.De Angelis[47], W.De Boer[17], C.De Clercq[2], B.De Lotto[47], N.De Maria[45], A.De Min[36], L.de Paula[48], L.Di Ciaccio[38], A.Di Simone[39], K.Doroba[52], J.Drees[53,8], M.Dris[32], G.Eigen[4], T.Ekelof[49], M.Ellert[49], M.Elsing[8], M.C.Espirito Santo[22], G.Fanourakis[11], D.Fassouliotis[11,3], M.Feindt[17], J.Fernandez[41], A.Ferrer[50], F.Ferro[13], U.Flagmeyer[53], H.Foeth[8], E.Fokitis[32], F.Fulda-Quenzer[20], J.Fuster[50], M.Gandelman[48], C.Garcia[50], Ph.Gavillet[8], E.Gazis[32], R.Gokieli[8,52], B.Golob[43], G.Gomez-Ceballos[41], P.Goncalves[22], E.Graziani[39], G.Grosdidier[20], K.Grzelak[52], J.Guy[37], C.Haag[17], A.Hallgren[49], K.Hamacher[53], K.Hamilton[35], S.Haug[33], F.Hauler[17], V.Hedberg[26], M.Hennecke[17], H.Herr[8], J.Hoffman[52], S-O.Holmgren[44], P.J.Holt[8], M.A.Houlden[23], K.Hultqvist[44], J.N.Jackson[23], G.Jarlskog[26], P.Jarry[40], D.Jeans[35], E.K.Johansson[44], P.D.Johansson[44], P.Jonsson[27], C.Joram[8], L.Jungermann[17], F.Kapusta[25], S.Katsanevas[27], E.Katsoufis[32], G.Kernel[43], B.P.Kersevan[8,43], U.Kerzel[17], A.Kiiskinen[15], B.T.King[23], N.J.Kjaer[8], P.Kluit[31], P.Kokkinias[11], C.Kourkoumelis[3], O.Kouznetsov[16], Z.Krumstein[16], M.Kucharczyk[18], J.Lamsa[1], G.Leder[51], F.Ledroit[14], L.Leinonen[44], R.Leitner[30], J.Lemonne[2], V.Lepeltier[20], T.Lesiak[18], W.Liebig[53], D.Liko[51], A.Lipniacka[44], J.H.Lopes[48], J.M.Lopez[34], D.Loukas[11], P.Lutz[40], L.Lyons[35], J.MacNaughton[51], A.Malek[53], S.Maltezos[32], F.Mandl[51], J.Marco[41], R.Marco[41], B.Marechal[48], M.Margoni[36], J-C.Marin[8], C.Mariotti[8], A.Markou[11], C.Martinez-Rivero[41], J.Masik[12], N.Mastroyiannopoulos[11], F.Matorras[41], C.Matteuzzi[29], F.Mazzucato[36], M.Mazzucato[36], R.Mc Nulty[23], C.Meroni[28], W.T.Meyer[1], E.Migliore[45], W.Mitaroff[51], U.Mjoernmark[26], T.Moa[44], M.Moch[17], K.Moenig[8,10], R.Monge[13], J.Montenegro[31], D.Moraes[48], S.Moreno[22], P.Morettini[13], U.Mueller[53], K.Muenich[53], M.Mulders[31], L.Mundim[6], W.Murray[37], B.Muryn[19], G.Myatt[35], T.Myklebust[33], M.Nassiakou[11], F.Navarria[5], K.Nawrocki[52], R.Nicolaidou[40], M.Nikolenko[16,9], A.Oblakowska-Mucha[19], V.Obraztsov[42], A.Olshevski[16], A.Onofre[22], R.Orava[15], K.Osterberg[15], A.Ouraou[40], A.Oyanguren[50], M.Paganoni[29], S.Paiano[5], J.P.Palacios[23], H.Palka[18], Th.D.Papadopoulou[32], L.Pape[8], C.Parkes[24], F.Parodi[13], U.Parzefall[8], A.Passeri[39], O.Passon[53], L.Peralta[22], V.Perepelitsa[50], A.Perrotta[5], A.Petrolini[13], J.Piedra[41], L.Pieri[39], F.Pierre[40], M.Pimenta[22], E.Piotto[8], T.Podobnik[43], V.Poireau[8], M.E.Pol[6], G.Polok[18], V.Pozdniakov[16], N.Pukhaeva[2,16], A.Pullia[29], J.Rames[12], L.Ramler[17], A.Read[33], P.Rebecchi[8], J.Rehn[17], D.Reid[31], R.Reinhardt[53], P.Renton[35], F.Richard[20], J.Ridky[12], M.Rivero[41], D.Rodriguez[41], A.Romero[45], P.Ronchese[36], E.Rosenberg[1], P.Roudeau[20], T.Rovelli[5], V.Ruhlmann-Kleider[40], D.Ryabtchikov[42], A.Sadovsky[16], L.Salmi[15], J.Salt[50], A.Savoy-Navarro[25], U.Schwickerath[8], A.Segar[35], R.Sekulin[37], M.Siebel[53], A.Sisakian[16], G.Smadja[27], O.Smirnova[26], A.Sokolov[42], A.Sopczak[21], R.Sosnowski[52], T.Spassov[8], M.Stanitzki[17], A.Stocchi[20], J.Strauss[51], B.Stugu[4], M.Szczekowski[52], M.Szeptycka[52], T.Szumlak[19], T.Tabarelli[29], A.C.Taffard[23], F.Tegenfeldt[49], J.Timmermans[31], L.Tkatchev[16], M.Tobin[23], S.Todorovova[12], B.Tome[22], A.Tonazzo[29], P.Tortosa[50], P.Travnicek[12], D.Treille[8], G.Tristram[7], M.Trochimczuk[52], C.Troncon[28], M-L.Turluer[40], I.A.Tyapkin[16], P.Tyapkin[16], S.Tzamarias[11], V.Uvarov[42], G.Valenti[5], P.Van Dam[31], J.Van Eldik[8], A.Van Lysebetten[2], N.van Remortel[2], I.Van Vulpen[8], G.Vegni[28], F.Veloso[22], W.Venus[37], P.Verdier[27], V.Verzi[38], D.Vilanova[40], L.Vitale[47], V.Vrba[12], H.Wahlen[53], A.J.Washbrook[23], C.Weiser[17], D.Wicke[8], J.Wickens[2], G.Wilkinson[35], M.Winter[9], M.Witek[18], O.Yushchenko[42], A.Zalewska[18], P.Zalewski[52], D.Zavrtanik[43], V.Zhuravlov[16], N.I.Zimin[16], A.Zintchenko[16], M.Zupan[11]

[1]Department of Physics and Astronomy, Iowa State University, Ames IA 50011-3160, USA
[2]Physics Department, Universiteit Antwerpen, Universiteitsplein 1, B-2610 Antwerpen, Belgium
and IIHE, ULB-VUB, Pleinlaan 2, B-1050 Brussels, Belgium
and Faculté des Sciences, Univ. de l'Etat Mons, Av. Maistriau 19, B-7000 Mons, Belgium
[3]Physics Laboratory, University of Athens, Solonos Str. 104, GR-10680 Athens, Greece
[4]Department of Physics, University of Bergen, Allégaten 55, NO-5007 Bergen, Norway
[5]Dipartimento di Fisica, Università di Bologna and INFN, Via Irnerio 46, IT-40126 Bologna, Italy
[6]Centro Brasileiro de Pesquisas Físicas, rua Xavier Sigaud 150, BR-22290 Rio de Janeiro, Brazil
and Depto. de Física, Pont. Univ. Católica, C.P. 38071 BR-22453 Rio de Janeiro, Brazil
and Inst. de Física, Univ. Estadual do Rio de Janeiro, rua São Francisco Xavier 524, Rio de Janeiro, Brazil
[7]Collège de France, Lab. de Physique Corpusculaire, IN2P3-CNRS, FR-75231 Paris Cedex 05, France
[8]CERN, CH-1211 Geneva 23, Switzerland
[9]Institut de Recherches Subatomiques, IN2P3 - CNRS/ULP - BP20, FR-67037 Strasbourg Cedex, France
[10]Now at DESY-Zeuthen, Platanenallee 6, D-15735 Zeuthen, Germany
[11]Institute of Nuclear Physics, N.C.S.R. Demokritos, P.O. Box 60228, GR-15310 Athens, Greece
[12]FZU, Inst. of Phys. of the C.A.S. High Energy Physics Division, Na Slovance 2, CZ-180 40, Praha 8, Czech Republic
[13]Dipartimento di Fisica, Università di Genova and INFN, Via Dodecaneso 33, IT-16146 Genova, Italy
[14]Institut des Sciences Nucléaires, IN2P3-CNRS, Université de Grenoble 1, FR-38026 Grenoble Cedex, France
[15]Helsinki Institute of Physics, P.O. Box 64, FIN-00014 University of Helsinki, Finland
[16]Joint Institute for Nuclear Research, Dubna, Head Post Office, P.O. Box 79, RU-101 000 Moscow, Russian Federation
[17]Institut für Experimentelle Kernphysik, Universität Karlsruhe, Postfach 6980, DE-76128 Karlsruhe, Germany
[18]Institute of Nuclear Physics,Ul. Kawiory 26a, PL-30055 Krakow, Poland
[19]Faculty of Physics and Nuclear Techniques, University of Mining and Metallurgy, PL-30055 Krakow, Poland
[20]Université de Paris-Sud, Lab. de l'Accélérateur Linéaire, IN2P3-CNRS, Bât. 200, FR-91405 Orsay Cedex, France
[21]School of Physics and Chemistry, University of Lancaster, Lancaster LA1 4YB, UK
[22]LIP, IST, FCUL - Av. Elias Garcia, 14-1^o, PT-1000 Lisboa Codex, Portugal
[23]Department of Physics, University of Liverpool, P.O. Box 147, Liverpool L69 3BX, UK
[24]Dept. of Physics and Astronomy, Kelvin Building, University of Glasgow, Glasgow G12 8QQ
[25]LPNHE, IN2P3-CNRS, Univ. Paris VI et VII, Tour 33 (RdC), 4 place Jussieu, FR-75252 Paris Cedex 05, France
[26]Department of Physics, University of Lund, Sölvegatan 14, SE-223 63 Lund, Sweden
[27]Université Claude Bernard de Lyon, IPNL, IN2P3-CNRS, FR-69622 Villeurbanne Cedex, France
[28]Dipartimento di Fisica, Università di Milano and INFN-MILANO, Via Celoria 16, IT-20133 Milan, Italy
[29]Dipartimento di Fisica, Univ. di Milano-Bicocca and INFN-MILANO, Piazza della Scienza 2, IT-20126 Milan, Italy
[30]IPNP of MFF, Charles Univ., Areal MFF, V Holesovickach 2, CZ-180 00, Praha 8, Czech Republic
[31]NIKHEF, Postbus 41882, NL-1009 DB Amsterdam, The Netherlands
[32]National Technical University, Physics Department, Zografou Campus, GR-15773 Athens, Greece
[33]Physics Department, University of Oslo, Blindern, NO-0316 Oslo, Norway
[34]Dpto. Fisica, Univ. Oviedo, Avda. Calvo Sotelo s/n, ES-33007 Oviedo, Spain
[35]Department of Physics, University of Oxford, Keble Road, Oxford OX1 3RH, UK
[36]Dipartimento di Fisica, Università di Padova and INFN, Via Marzolo 8, IT-35131 Padua, Italy
[37]Rutherford Appleton Laboratory, Chilton, Didcot OX11 OQX, UK
[38]Dipartimento di Fisica, Università di Roma II and INFN, Tor Vergata, IT-00173 Rome, Italy
[39]Dipartimento di Fisica, Università di Roma III and INFN, Via della Vasca Navale 84, IT-00146 Rome, Italy
[40]DAPNIA/Service de Physique des Particules, CEA-Saclay, FR-91191 Gif-sur-Yvette Cedex, France
[41]Instituto de Fisica de Cantabria (CSIC-UC), Avda. los Castros s/n, ES-39006 Santander, Spain
[42]Inst. for High Energy Physics, Serpukov P.O. Box 35, Protvino, (Moscow Region), Russian Federation
[43]J. Stefan Institute, Jamova 39, SI-1000 Ljubljana, Slovenia and Laboratory for Astroparticle Physics,
Nova Gorica Polytechnic, Kostanjeviska 16a, SI-5000 Nova Gorica, Slovenia,
and Department of Physics, University of Ljubljana, SI-1000 Ljubljana, Slovenia
[44]Fysikum, Stockholm University, Box 6730, SE-113 85 Stockholm, Sweden
[45]Dipartimento di Fisica Sperimentale, Università di Torino and INFN, Via P. Giuria 1, IT-10125 Turin, Italy
[46]INFN,Sezione di Torino, and Dipartimento di Fisica Teorica, Università di Torino, Via P. Giuria 1,
IT-10125 Turin, Italy
[47]Dipartimento di Fisica, Università di Trieste and INFN, Via A. Valerio 2, IT-34127 Trieste, Italy
and Istituto di Fisica, Università di Udine, IT-33100 Udine, Italy
[48]Univ. Federal do Rio de Janeiro, C.P. 68528 Cidade Univ., Ilha do Fundão BR-21945-970 Rio de Janeiro, Brazil
[49]Department of Radiation Sciences, University of Uppsala, P.O. Box 535, SE-751 21 Uppsala, Sweden
[50]IFIC, Valencia-CSIC, and D.F.A.M.N., U. de Valencia, Avda. Dr. Moliner 50, ES-46100 Burjassot (Valencia), Spain
[51]Institut für Hochenergiephysik, Österr. Akad. d. Wissensch., Nikolsdorfergasse 18, AT-1050 Vienna, Austria
[52]Inst. Nuclear Studies and University of Warsaw, Ul. Hoza 69, PL-00681 Warsaw, Poland
[53]Fachbereich Physik, University of Wuppertal, Postfach 100 127, DE-42097 Wuppertal, Germany

1 Introduction

Flavour Changing Neutral Currents (FCNC) are highly suppressed in the Standard Model (SM) due to the Glashow-Iliopoulos-Maiani (GIM) mechanism [1]. However, small contributions appear at one-loop level ($\mathrm{Br}(t \to (\gamma, g, Z) + c(u)) < 10^{-10}$) due to the Cabibbo-Kobayashi-Maskawa (CKM) mixing matrix [2]. Many extensions of the SM, such as supersymmetry [3] and multi-Higgs doublet models [4], predict the presence of FCNC already at tree level. Some specific models [5] give rise to detectable FCNC amplitudes.

The most prominent signature for direct observation of FCNC processes at LEP is the production of a top quark together with a charm or an up quark in the process $e^+e^- \to t\bar{c}$ [1]. The strength of the transitions $\gamma \to \mathrm{ff'}$ and $Z \to \mathrm{ff'}$ can be described in terms of the Lagrangian given in [6]:

$$\Gamma_\mu^\gamma = \kappa_\gamma \frac{ee_q}{\Lambda} \sigma_{\mu\nu} \left(g_1 P_l + g_2 P_r\right) q^\nu, \tag{1}$$

$$\Gamma_\mu^Z = \kappa_Z \frac{e}{\sin 2\Theta_W} \gamma_\mu \left(z_1 P_l + z_2 P_r\right), \tag{2}$$

where e is the electron charge, e_q the top quark charge, Θ_W is the weak mixing angle and P_l (P_r) is the left (right) handed projector. The κ_γ and κ_Z are the anomalous couplings to the γ and Z bosons, respectively. Λ is the new physics scale. A value of 175 GeV was used for numerical calculations throughout the paper. The relative contributions of the left and right handed currents are determined by the g_i and z_i constants which obey the constraints:

$$g_1^2 + g_2^2 = 1, \quad z_1^2 + z_2^2 = 1. \tag{3}$$

In the approach which gives the most conservative limits on the couplings, the interference term, which depends on g_i and z_i, gives a negative contribution to the cross-section of the process $e^+e^- \to t\bar{c}$. This corresponds to the requirement [6]:

$$g_1 z_1 + g_2 z_2 = -1. \tag{4}$$

The existence of anomalous top couplings to gauge bosons allows the top to decay through $t \to c\gamma$ and $t \to cZ$ in addition to the dominant decay mode $t \to bW$. This effect was taken into account in the evaluation of results. Numerical estimates of the expected number of events taking into account the limits on anomalous vertices set by the CDF collaboration [7] can be found in [6].

This paper is devoted to the search for FCNC processes associated to single top production at LEP ($e^+e^- \to t\bar{c}$). Limits are set on the anomalous couplings κ_γ and κ_Z in the most conservative approach. The t quark is expected to decay predominantly into Wb, giving distinct signatures for the leptonic and hadronic W decays. For each decay mode a dedicated analysis was developed. In the *semileptonic channel* two jets and one isolated lepton (from the W leptonic decays, $W \to l\nu_l$) were searched for. In the *hadronic channel* four jets were required in the event (two of them from the W hadronic decays, $W \to qq'$). A nearly background-free signature is obtained in the semileptonic channel, but the branching ratio is relatively low. In the hadronic channel, the W decays give an event rate about two times higher, but the background conditions are less favourable.

[1]Throughout this paper the notation $t\bar{c}$ stands for $t\bar{c}$+$t\bar{u}$ and includes the charge conjugate contribution as well.

2 The DELPHI data and simulated samples

The data collected with the DELPHI detector [8] at $\sqrt{s} = 189 - 208$ GeV, well above the $t\bar{c}$ production threshold, were used in this analysis. The integrated luminosity used for each centre-of-mass energy bin is given in Table 1. The data collected in the year 2000 at energies up to 208 GeV are split into two energy bins 205 GeV and 207 GeV for centre-of-mass energies below and above 206 GeV, respectively. The 189, 192, 196, 200, 202, 205 and 207 GeV energy bins correspond to average centre-of-mass energies of 188.6, 191.6, 195.5, 199.5, 201.6, 204.8 and 206.6 GeV, respectively. While for the semileptonic channel the two last energy bins were considered separately, they were considered together in the hadronic channel.

The background process $e^+e^- \rightarrow Z/\gamma \rightarrow q\bar{q}(\gamma)$ was generated with PYTHIA 6.125 [9]. For $\mu^+\mu^-(\gamma)$ and $\tau^+\tau^-(\gamma)$, DYMU3 [10] and KORALZ 4.2 [11] were used, respectively, while the BHWIDE generator [12] was used for Bhabha events. Simulation of four-fermion final states was performed using EXCALIBUR [13] and GRC4F [14]. Two-photon interactions giving hadronic final states were generated using TWOGAM [15]. Signal events were generated by a standalone simulation program interfaced with PYTHIA 6.125 [9] for quark hadronization. The generation of the signal events was performed with radiative corrections included. The SM contribution is known to be very small ($\mathrm{Br}(t \rightarrow (\gamma, g, Z)+c(u)) < 10^{-10}$ [2]) and was not taken into account. Both the signal and background events were passed through the detailed simulation of the DELPHI detector and then processed with the same reconstruction and analysis programs as the real data.

$\sqrt{s}$ (GeV)	189	192	196	200	202	205	207
Luminosity (pb $^{-1}$)	151.8	25.9	76.4	83.4	40.1	78.8	84.3

Table 1: Luminosity collected by DELPHI and used in this analysis for each centre-of-mass energy (see text for details).

3 Hadronic channel

In the hadronic channel, the final state corresponding to the single top production is characterized by four jets: a b jet from the top decay, a spectator c jet and two other jets from the W hadronic decay.

In this analysis the reconstructed charged particle tracks were required to fulfil the following criteria[2]:

- momentum $p > 0.4$ GeV/c;
- momentum error $\Delta p/p < 1$;
- $R\phi$ impact parameter < 4 cm;
- z impact parameter < 10 cm.

Tracks seen by only the central tracking devices (Vertex Detector and Inner Detector) were rejected. Neutral clusters were required to have an energy of at least 400 MeV.

[2] The DELPHI coordinate system has the z-axis aligned along the electron beam direction, the x-axis pointing toward the centre of LEP and y-axis vertical. R is the radius in the (x, y) plane. The polar angle Θ is measured with respect to the z-axis and the azimuthal angle ϕ is about z.

Events with the visible energy > 100 GeV and at least 8 charged tracks were selected for further processing.

The information of the DELPHI calorimeters and tracking devices was used to classify charged particles as electrons or muons according to standard DELPHI algorithms [8]. A well-identified lepton was designated as a "standard" lepton. Whenever some ambiguity persisted the lepton was called a "loose" lepton. To each lepton tag there corresponds a given detection efficiency and misidentification probability [8]. Events with leptons with momenta above 20 GeV/c, identified as at least "standard" electrons or "loose" muons, were rejected.

The LUCLUS [9] algorithm with $d_{join} = 6.5$ GeV/c was then applied to cluster the event into jets. Events with 4, 5, or 6 jets were selected and forced into a 4-jet topology. Each of the three most energetic jets must contain at least one charged particle. The preselection was completed by requiring the event visible energy and combined b-tag parameter [16] to be greater than 130 GeV and -1.5, respectively. The energies and momenta of the jets were then rescaled by applying a constrained fit with NDF $= 4$ imposing four-momentum conservation [17].

The assignment of jets to quarks is not straightforward as the kinematics of the event varies strongly with the energy. Near the $t\bar{c}$ production threshold both quarks are produced at rest and the subsequent top decay ($t \to Wb$) produces a high momentum b quark. However, at higher LEP centre-of-mass energies the c quark becomes more energetic with momentum values up to 30 GeV/c. Four different methods of jet assignment were considered:

1. the jet with highest b-tag parameter [16] was the b jet candidate and the least energetic jet (among the three remaining jets) was the c jet candidate;
2. the most energetic jet was the b jet candidate and the least energetic one was the c jet candidate;
3. the jet with highest b-tag parameter was the b jet candidate and two jets were assigned to the W according to the probability of the 5-C constrained fit;
4. the most energetic jet was the b jet candidate and two jets were assigned to the W according to the probability of the 5-C constrained fit.

All the above studies were performed and the highest efficiency for the signal and strongest background suppression was obtained with the first method. This method was used in the hadronic analysis for all centre-of-mass energies. Method (2), well suited at the kinematic threshold of single-top production, was less efficient at the highest LEP energies because the energy of the b jet becomes comparable to the energies of the other jets.

After the preselection, signal and background-like probabilities were assigned to each event based on Probability Density Functions (PDF) constructed with the following variables:

- the event thrust value [18];
- the event sphericity [18];
- the event b-tag calculated with the combined algorithm [16];
- the energy of the jet assigned as b jet (E_b);
- the energy of the most energetic jet in the event (E_{max});
- the ratio of the energies of the least and most energetic jets (E_{min}/E_{max});
- the invariant mass of the two jets assigned as originating from the W decay (M_W);
- the absolute value of the reconstructed W momentum (P_W).

Examples of these distributions are shown in figures 1 and 2, after the preselection.

All eight PDF were estimated for the signal ($\mathcal{P}_i^{signal}$) and background ($\mathcal{P}_i^{back}$) distributions. They were used to construct the signal $\mathcal{L_S}=\prod_{i=1}^{8}\mathcal{P}_i^{signal}$ and background $\mathcal{L_B}=\prod_{i=1}^{8}\mathcal{P}_i^{back}$ likelihoods. A discriminant variable

$$W = \ln(\mathcal{L_S}/\mathcal{L_B}) \tag{5}$$

based on the ratio of the likelihoods was then constructed for each event.

Figure 3 shows the discriminant variable distribution and the number of accepted events, at $\sqrt{s} = 205 - 207$ GeV, as function of signal efficiency for a top mass of 175 GeV/c^2. Events were selected by applying a cut on the discriminant variable $\ln(\mathcal{L_S}/\mathcal{L_B})$, dependent on the centre-of-mass energy. Its value was chosen to maximize the efficiency for a low background contamination. The number of data events and expected background from the SM processes (mostly WW background) passing the likelihood ratio selection are shown in Table 2 for all centre-of-mass energies, together with the signal efficiencies convoluted with the W hadronic branching ratio. A general good agreement with the Standard Model expectations is observed.

$\sqrt{s}$	Preselection		Final Selection		
(GeV)	Data	Back. ± stat.	Data	Back.±stat.±syst.	$\epsilon \times Br.$ (%)
189	568	530.6 ± 3.3	37	37.1 ± 1.4 ± 1.2	17.6 ± 0.5 ± 0.4
192	106	91.4 ± 1.2	3	3.4 ± 0.4 ± 0.3	17.7 ± 0.5 ± 0.4
196	266	253.1 ± 1.5	17	10.7 ± 0.4 ± 0.4	17.9 ± 0.6 ± 0.5
200	251	265.0 ± 1.7	12	11.9 ± 0.5 ± 0.7	16.7 ± 0.5 ± 0.4
202	134	133.3 ± 0.9	5	6.9 ± 0.3 ± 0.3	17.9 ± 0.6 ± 0.5
205 − 207	486	544.1 ± 2.7	25	30.1 ± 0.9 ± 1.2	17.5 ± 0.5 ± 0.6

Table 2: Number of events in the hadronic analysis at the preselection and final selection levels, for different centre-of-mass energies. The efficiencies convoluted with the W hadronic branching ratio (Br) are shown for a top-quark mass of 175 GeV/c^2. Statistical and systematic errors are also given (see section 5).

4 Semileptonic channel

In the semileptonic channel, the final state corresponding to single top production is characterized by two jets (a b jet from the top decay and a spectator c jet) and at least one isolated lepton from the W leptonic decay.

At the preselection level, events with an energy in the detector greater than 20% of the centre-of-mass energy and at least 7 charged particles were selected. The identification of muons relies on the association of charged particles to signals in the muon chambers and in the hadronic calorimeter and was provided by standard DELPHI algorithms [8].

The identification of electrons and photons was performed by combining information from the electromagnetic calorimeter and the tracking system. Radiation and interaction effects were taken into account by an angular clustering procedure around the main shower [19].

Isolated leptons (photons) were defined by constructing double cones centered around the axis of the charged particle track (neutral cluster) with half-opening angles of 5° and

25° (5° and 15°), and requiring that the average energy density in the region between the two cones was below 150 MeV/degree (100 MeV/degree), to assure isolation. In the case of neutral deposits, no charged particle with more than 250 MeV/c was allowed inside the inner cone. The energy of the isolated particle was then re-evaluated as the sum of the energies inside the inner cone. For well identified leptons or photons the above requirements were weakened. In this case only the external cone was used and the angle α was varied according to the energy of the lepton (photon) candidate, down to 2° for $P_{lep} \geq 70$ GeV/c (3° for $E_\gamma \geq 90$ GeV), with the allowed energy inside the cone reduced by $\sin\alpha/\sin 25^\circ$ ($\sin\alpha/\sin 15^\circ$).

Events with only one charged lepton and no isolated photons were selected. No other specific criteria were additionally applied to perform lepton flavour identification.

All other particles were then forced into jets using the Durham jet algorithm [20], which is based on a scaled transverse momentum method. Two-jet events were selected by a cut on the value of the corresponding resolution variable y at the transition between one and two jets: $-log_{10}(y_{2\rightarrow1}) \geq 0.45$. The most energetic particle in each jet had to be charged. It was required that the momenta of the lepton and jets were greater than 10 GeV/c and 5 GeV/c, respectively. Polar angles of the lepton and of the two jets were required to be in the region $20^\circ \leq \theta_{lep} \leq 160^\circ$ and $10^\circ \leq \theta_{j1,j2} \leq 170^\circ$, respectively. The missing momentum polar angle had to be above 20° and below 160° and the combined b-tag parameter [16] of the most energetic jet was required to be greater than -1.1.

The energies and momenta of the jets, the lepton and the momentum of the undetected neutrino (assumed to be the missing momentum) were calculated from four-momentum conservation with a constrained fit (NDF=1). Events with χ^2 lower than 7 were accepted, provided the invariant mass of the neutrino and the isolated lepton was below 125 GeV/c^2. The most energetic jet was assigned to the b quark and the second jet to the c quark. The top mass was reconstructed as the invariant mass of the b jet, the isolated lepton and the neutrino four-momenta.

Figures 4 and 5 show some relevant distributions for data and MC, after the preselection and for $\sqrt{s} = 205-207$ GeV. The number of events at preselection and final selection levels are given in Table 3 for each centre-of-mass energy. Most of the background comes from SM $e^+e^- \rightarrow WW$ events.

After the preselection, signal and background-like probabilities were assigned to each event (as for the hadronic channel) based on PDF constructed with the following variables:

- momentum of the less energetic jet;
- more energetic jet b-tag variable [16];
- reconstructed mass of the two jets;
- reconstructed top mass;
- angle between the two jets;
- lepton-neutrino invariant mass;
- $q_l \cdot \cos\theta_l$, where q_l is the charge and θ_l is the polar angle of the lepton;
- $q_{j1} \cdot \cos\theta_{j1}$, where $q_{j1} = -q_l$ and θ_{j1} is the polar angle of the more energetic jet;
- $p_{j1} \cdot [\sqrt{s} - p_{j1}(1 - \cos\theta_{j1\,j2})]$, where p_{j1} is the momentum of the more energetic jet and $\theta_{j1\,j2}$ is the angle between the two jets. This variable is proportional to $(m_t^2 - m_W^2)/2$. i.e., not dependent on the centre-of-mass energy.

The signal ($\mathcal{L_S}$) and background ($\mathcal{L_B}$) likelihoods were used on an event-by-event basis to compute a discriminant variable defined as $\ln(\mathcal{L_S}/\mathcal{L_B})$. A loose cut on the signal likelihood was applied to the events. Figure 6 presents, after this cut, the discriminant variable distribution and the number of events accepted as a function of signal efficiency

for $\sqrt{s}$=205-207 GeV (assuming a top mass of 175 GeV/c^2 for the signal). There is a general good agreement between the data and the SM predictions. The background distribution has a tail for higher values of the discriminant variable which goes below every data event. Correlations between the variables were studied. Their effect on the likelihood ratio is small.

Events were further selected by applying a cut on the discriminant variable $\ln(\mathcal{L}_\mathcal{S}/\mathcal{L}_\mathcal{B})$, dependent on the centre-of-mass energy. Table 3 shows the number of data and background events which passed the cut for the different centre-of-mass energies. The efficiencies convoluted with the W leptonic branching ratio are also shown. The dominant backgrounds come from SM $e^+e^- \to WW$ and $e^+e^- \to\ q\bar{q}$ events.

$\sqrt{s}$ (GeV)	Preselection		Final Selection		
	Data	Back. $\pm$ stat.	Data	Back.$\pm$stat.$\pm$syst.	$\epsilon \times Br.$ (%)
189	102	120.7 $\pm$ 4.3	1	2.4 $\pm$ 0.7 $\pm$ 0.8	8.0 $\pm$ 0.3 $\pm$ 0.5
192	24	21.5 $\pm$ 0.8	1	0.5 $\pm$ 0.1 $\pm$ 0.1	7.7 $\pm$ 0.9 $\pm$ 0.5
196	72	76.2 $\pm$ 2.5	2	0.9 $\pm$ 0.3 $\pm$ 0.1	7.1 $\pm$ 0.9 $\pm$ 0.5
200	95	87.6 $\pm$ 2.8	1	2.0 $\pm$ 0.5 $\pm$ 0.3	6.9 $\pm$ 0.3 $\pm$ 0.3
202	40	42.2 $\pm$ 1.3	1	1.7 $\pm$ 0.3 $\pm$ 0.1	7.9 $\pm$ 0.4 $\pm$ 0.3
205	90	90.0 $\pm$ 2.9	2	1.4 $\pm$ 0.4 $\pm$ 0.1	6.2 $\pm$ 0.3 $\pm$ 0.3
207	71	90.2 $\pm$ 2.6	2	1.9 $\pm$ 0.5 $\pm$ 0.2	6.2 $\pm$ 0.3 $\pm$ 0.4

Table 3: Number of events in the semileptonic analysis at the preselection and final selection levels, for the different centre-of-mass energies. The efficiencies convoluted with the W leptonic branching ratio are also shown for a top mass of 175 GeV/c^2. Statistical and systematic errors are given (see the systematic errors and limit derivation section).

5 Systematic errors and limit derivation

Studies of systematic errors were performed and their effect evaluated at the final selection level. The stability of the results with respect to variations on the selection criteria, the PDF definition, the different hadronization schemes and the uncertainty in top quark mass were studied.

Concerning the stability of the results, an independent (and large, compared to the resolution) variation on the selection criteria applied to analysis variables like the missing momentum polar angle, the combined b-tag of the most energetic jet, the W mass, the Durham resolution variable, etc. was allowed. The most significant contributions gave a maximum error of 0.5 events and 0.3% for the expected background and efficiency, respectively. Different smoothing procedures were performed for the PDF definition and their effect is at most 0.5 events (0.4%) for the expected background (signal efficiency). Different hadronization schemes (string and independent) [9] were studied for the signal and their effect contributes at most 0.1% for the signal efficiency error. The uncertainty on the top quark mass is the most important source of systematic errors. It affects not only the total production cross-section but also the kinematics of signal events. In terms of signal efficiency, its effect could be as high as 0.9% for the semileptonic channel (in the mass range between 170 GeV/c^2 and 180 GeV/c^2). The effects of such variations (added

quadratically) on the final selection criteria are quoted as a systematic error in Tables 2 and 3.

The number of data and expected SM background events for the hadronic and semileptonic channels, the respective signal efficiencies and data luminosity collected at the various centre-of-mass energies were combined to derive limits in the (κ_γ, κ_Z) plane using a Bayesian approach [21]. In total, 13 independent channels (6 in the hadronic and 7 in the semileptonic modes) correspond to different $\sqrt{s}$ values. These channels are fitted simultaneously to extract the limits on the FCNC parameters. The total production cross-section and top FCNC decay widths dependence with κ_γ and κ_Z were properly considered [6] in the limit derivation.

The effect of systematic errors on the $(\kappa_\gamma, \kappa_Z)$ plane limits was considered. Initial State Radiation (ISR) and QCD corrections [22] were also taken into account in the $t\bar{c}$ total production cross-section.

Figure 7 shows the 95% confidence level (C.L.) upper limits in the (κ_γ, κ_Z) plane obtained by this analysis. The different filled areas correspond to the allowed regions obtained for different top mass values and $\Lambda = 175$ GeV. Due to the s-channel Z dominance, the LEP2 data are less sensitive to the κ_γ parameter than to κ_Z. The upper limits obtained by the CDF collaboration [7] and ZEUS [23] are also shown in the figure for comparison. The 95% C.L. upper limits on each coupling parameter, setting the other coupling to zero, are summarized in Table 4. For comparison the values at $m_t = 175$ GeV/c^2 are $\kappa_Z(\kappa_\gamma = 0) = 0.434$ and $\kappa_\gamma(\kappa_Z = 0) = 0.505$ if the Born level cross-section (without radiative corrections) is taken into account.

m_t (GeV/c^2)	170	175	180
$\kappa_Z(\kappa_\gamma = 0)$	0.340	0.411	0.527
$\kappa_\gamma(\kappa_Z = 0)$	0.402	0.486	0.614

Table 4: 95% C.L. upper limits derived from the combined hadronic and semileptonic channels at $\sqrt{s} = 189 - 208$ GeV for $\Lambda = 175$ GeV.

Upper limits were also obtained by using only the hadronic and the semileptonic channels separately when radiative corrections to the total production cross-section were taken into account. The values at $m_t = 175$ GeV/c^2 are $\kappa_Z(\kappa_\gamma = 0) = 0.491$ (0.547) and $\kappa_\gamma(\kappa_Z = 0) = 0.568$ (0.625) for the hadronic (semileptonic) channel alone.

6 Summary

The data collected by the DELPHI detector at centre-of-mass energies ranging from 189 to 208 GeV were used to perform a search for FCNC $t\bar{c}$ production, in the hadronic and semileptonic topologies. No deviation with respect to the SM expectations was found. Upper limits on the anomalous couplings κ_γ and κ_Z were derived. A comparison with CDF [7] and ZEUS [23] is also shown. Results on the search for single-top production were also obtained by the other experiments at LEP [24].

Acknowledgements

We are greatly indebted to our technical collaborators, to the members of the CERN-SL Division for the excellent performance of the LEP collider, and to the funding agencies for their support in building and operating the DELPHI detector.
We acknowledge in particular the support of
Austrian Federal Ministry of Education, Science and Culture, GZ 616.364/2-III/2a/98,
FNRS–FWO, Flanders Institute to encourage scientific and technological research in the industry (IWT), Federal Office for Scientific, Technical and Cultural affairs (OSTC), Belgium,
FINEP, CNPq, CAPES, FUJB and FAPERJ, Brazil,
Czech Ministry of Industry and Trade, GA CR 202/99/1362,
Commission of the European Communities (DG XII),
Direction des Sciences de la Matière, CEA, France,
Bundesministerium für Bildung, Wissenschaft, Forschung und Technologie, Germany,
General Secretariat for Research and Technology, Greece,
National Science Foundation (NWO) and Foundation for Research on Matter (FOM), The Netherlands,
Norwegian Research Council,
State Committee for Scientific Research, Poland, SPUB-M/CERN/PO3/DZ296/2000, SPUB-M/CERN/PO3/DZ297/2000 and 2P03B 104 19 and 2P03B 69 23(2002-2004)
JNICT–Junta Nacional de Investigação Científica e Tecnológica, Portugal,
Vedecka grantova agentura MS SR, Slovakia, Nr. 95/5195/134,
Ministry of Science and Technology of the Republic of Slovenia,
CICYT, Spain, AEN99-0950 and AEN99-0761,
The Swedish Natural Science Research Council,
Particle Physics and Astronomy Research Council, UK,
Department of Energy, USA, DE-FG02-01ER41155,
EEC RTN contract HPRN-CT-00292-2002.

References

[1] S.L. Glashow, J. Iliopoulos, L. Maiani, *Phys. Rev.* **D 2** (1970) 1285.

[2] B. Grzadkowski, J.F. Gunion, P. Krawczyk, *Phys. Lett.* **B 268** (1991) 106;
G. Eilam, J.L. Hewett, A. Soni, *Phys. Rev.* **D 44** (1991) 1473 and *Erratum ibid* **D 59** (1999) 039901;
M.E. Luke, M.J. Savage, *Phys Lett.* **B 307** (1993) 387.

[3] G.M. de Divitiis, R. Petronzio, L. Silvestrini, *Nucl. Phys.* **B 504** (1997) 45.

[4] D. Atwood, L. Reina, A. Soni, *Phys. Rev.* **D 53** (1996) 1199.

[5] B.A. Arbuzov, M.Yu. Osipov, *Phys. Atom. Nucl.* **62** (1999) 485,
Yad. Fiz. **62** (1999) 528.

[6] V.F. Obraztsov, S.R. Slabospitsky, O.P. Yushchenko, *Phys. Lett.* **B 426** (1998) 393.

[7] CDF Coll., F. Abe et al., *Phys. Rev. Lett.* **80** (1998) 2525.

[8] DELPHI Coll., P. Aarnio et al., *Nucl. Instr. Meth.* **A 303** (1991) 233;
DELPHI Coll., P. Abreu et al., *Nucl. Instr. Meth.* **A 378** (1996) 57.

[9] T. Sjöstrand, *Comp. Phys. Comm.* **82** (1994) 74.

[10] J.E. Campagne, R. Zitoun, *Zeit. Phys.* **C 43** (1989) 469.

[11] S. Jadach, B.F.L. Ward, Z. Was, *Comp. Phys. Comm.* **79** (1994) 503.

[12] S. Jadach, W. Placzek, B.F.L. Ward, *Phys. Lett.* **B 390** (1997) 298.

[13] F.A. Berends, R. Pittau, R. Kleiss, *Comp. Phys. Comm.* **85** (1995) 437.

[14] J. Fujimoto et al., *Comp. Phys. Comm.* **100** (1997) 128.

[15] T. Alderweireld et al., CERN-2000-009, p. 219.

[16] DELPHI Coll., J. Abdallah et al. *"b-tagging in DELPHI at LEP"*, CERN-EP/2002-088 (submitted to *Eur. Phys. J.***C**)

[17] DELPHI Coll., P.Abreu et al., *Eur. Phys. J.* **C2** (1998) 581.

[18] DELPHI Coll., P. Abreu et al., *Zeit. Phys.* **C 73** (1996) 11.

[19] F. Cossutti, A. Tonazzo, F. Mazzucato, *"REMCLU: a package for the Reconstruction of Electromagnetic CLUsters at LEP200"*, DELPHI note 2000-164 (2000).

[20] S. Catani et al., *Phys. Lett.* **B 269** (1991) 432.

[21] V.F. Obraztsov, *Nucl. Instr. Meth.* **A 316** (1992) 388
and *Erratum* in *Nucl. Instr. Meth.* **A 399** (1997) 500.

[22] L.J. Reinders, H. Rubinstein and S. Yazaki, *Phys. Rep.* **127** (1985) 1.

[23] ZEUS Coll., S. Chekanov, *Phys. Lett.***B 559** (2003) 153.

[24] ALEPH Coll., A. Heister et al., *Phys. Lett.* **B 543** (2002) 173;
OPAL Coll., G. Abbiendi et al., *Phys. Lett.* **B 521** (2001) 181;
L3 Coll., P. Achard et al., *Phys. Lett.* **B 549** (2002) 290.

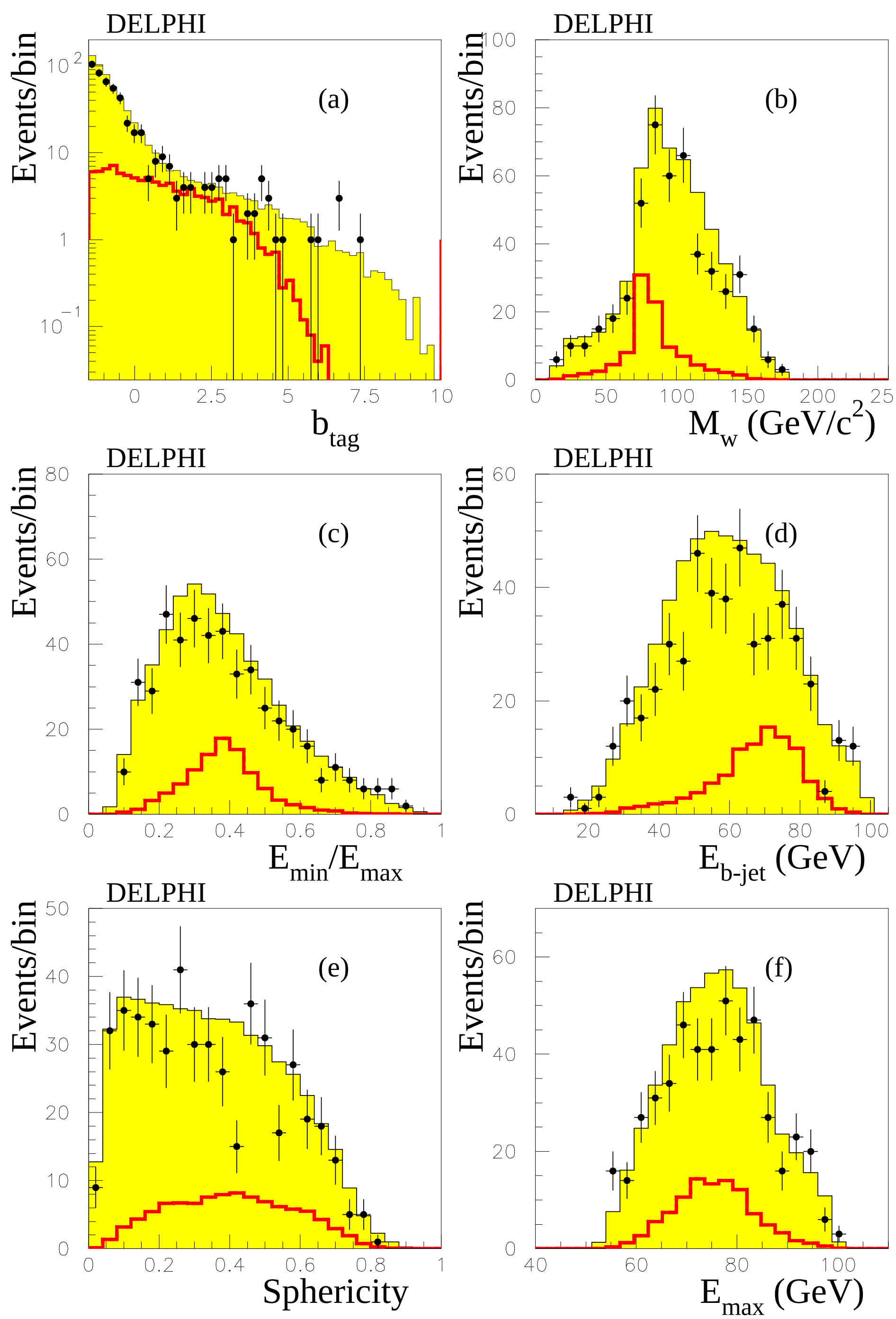

Figure 1: Distributions of relevant variables for the hadronic decay channel after the preselection, for $\sqrt{s} = 205 - 207$ GeV: (a) the b-tag variable, (b) the reconstructed W mass, (c) the ratio between the minimal and the maximal jet energies, (d) the energy of the most b-like jet, (e) the sphericity of the event and (f) the energy of the most energetic jet. The dots show the data, the shaded region the SM simulation and the thick line the expected signal behaviour (with arbitrary normalization) for a top mass of 175 GeV/c^2.

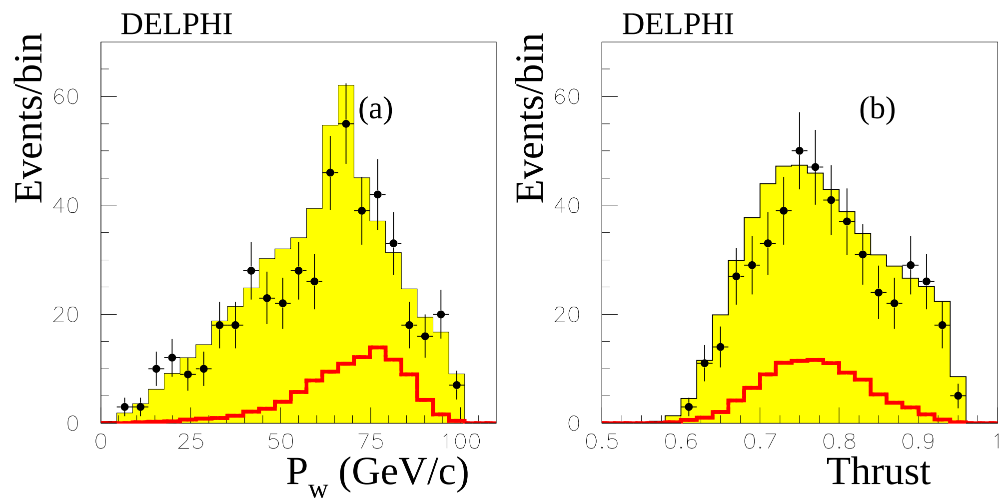

Figure 2: Distributions of relevant variables for the hadronic decay channel after the preselection for $\sqrt{s} = 205 - 207$ GeV: (a) the reconstructed W momentum and (b) the event thrust. The dots show the data and the shaded histograms show the SM simulation. The signal distribution with an arbitrary normalization is shown by the thick line for a top quark mass of 175 GeV/c^2.

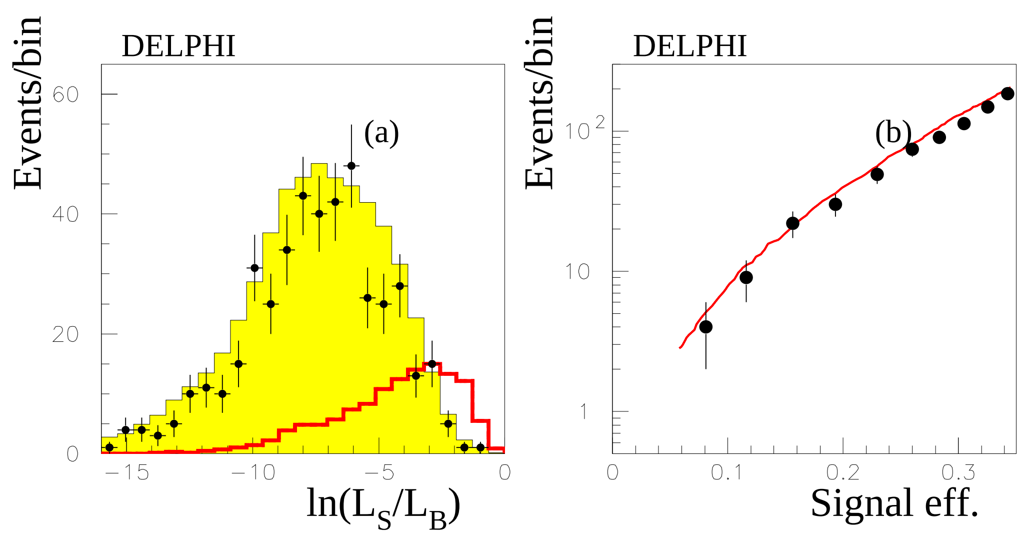

Figure 3: (a) distributions of the discriminant variable at $\sqrt{s} = 205 - 207$ GeV for data (dots), SM background simulation (shadowed region) and signal (thick line) with arbitrary normalization and (b) number of accepted data events (dots) together with the expected SM background simulation (full line) as a function of the signal efficiency (convoluted with the W hadronic branching ratio) for a top mass of 175 GeV/c^2.

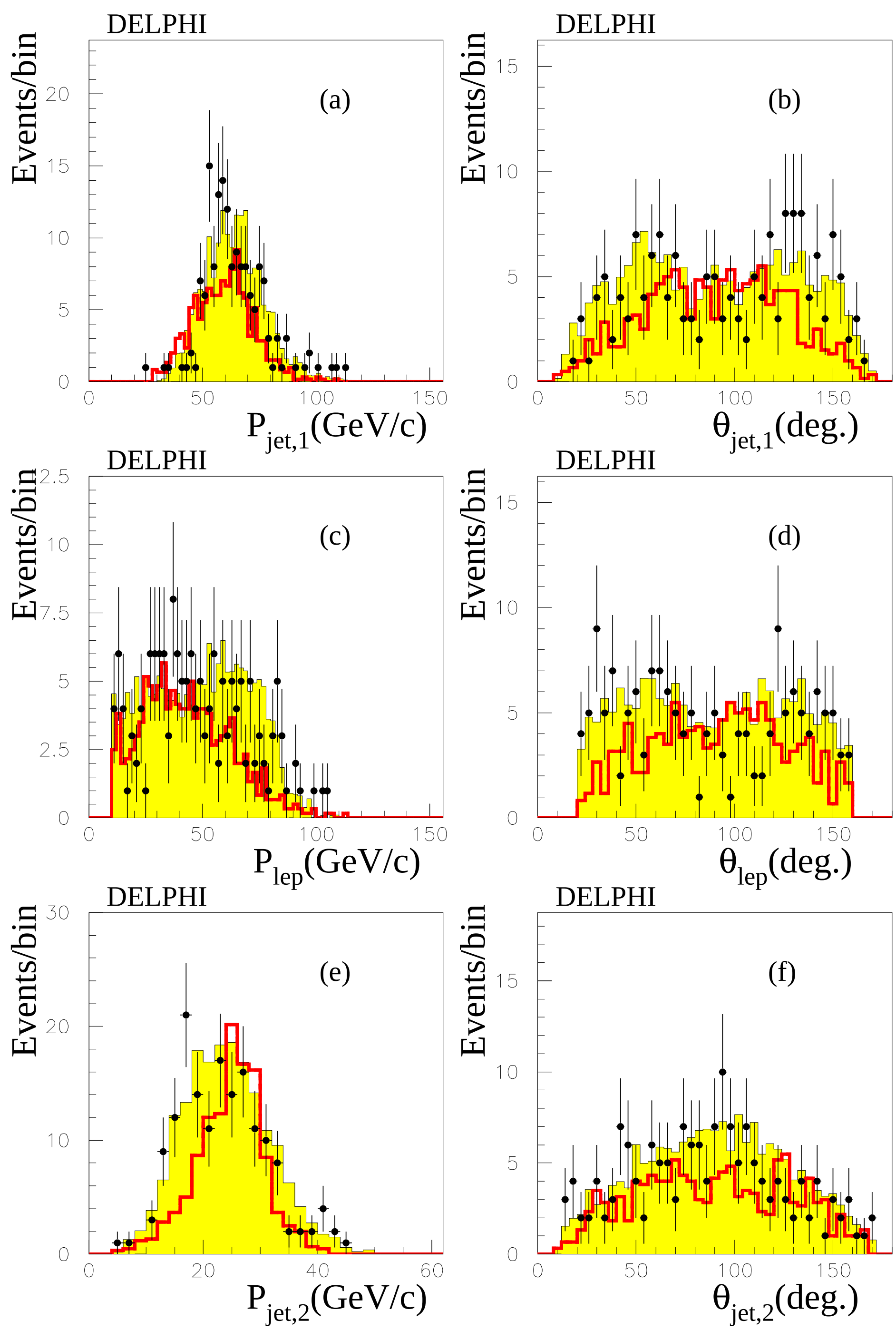

Figure 4: Distributions of relevant variables for the semileptonic decay channel at the preselection level for $\sqrt{s} = 205 - 207$ GeV. The momentum of the most energetic jet (a) and its polar angle (b), the lepton momentum (c) and its polar angle (d), the momentum of the least energetic jet (e) and its polar angle (f) are shown. The dots show the data, the shaded region the SM simulation and the thick line the expected signal behaviour (with arbitrary normalization) for a top mass of 175 GeV/c^2.

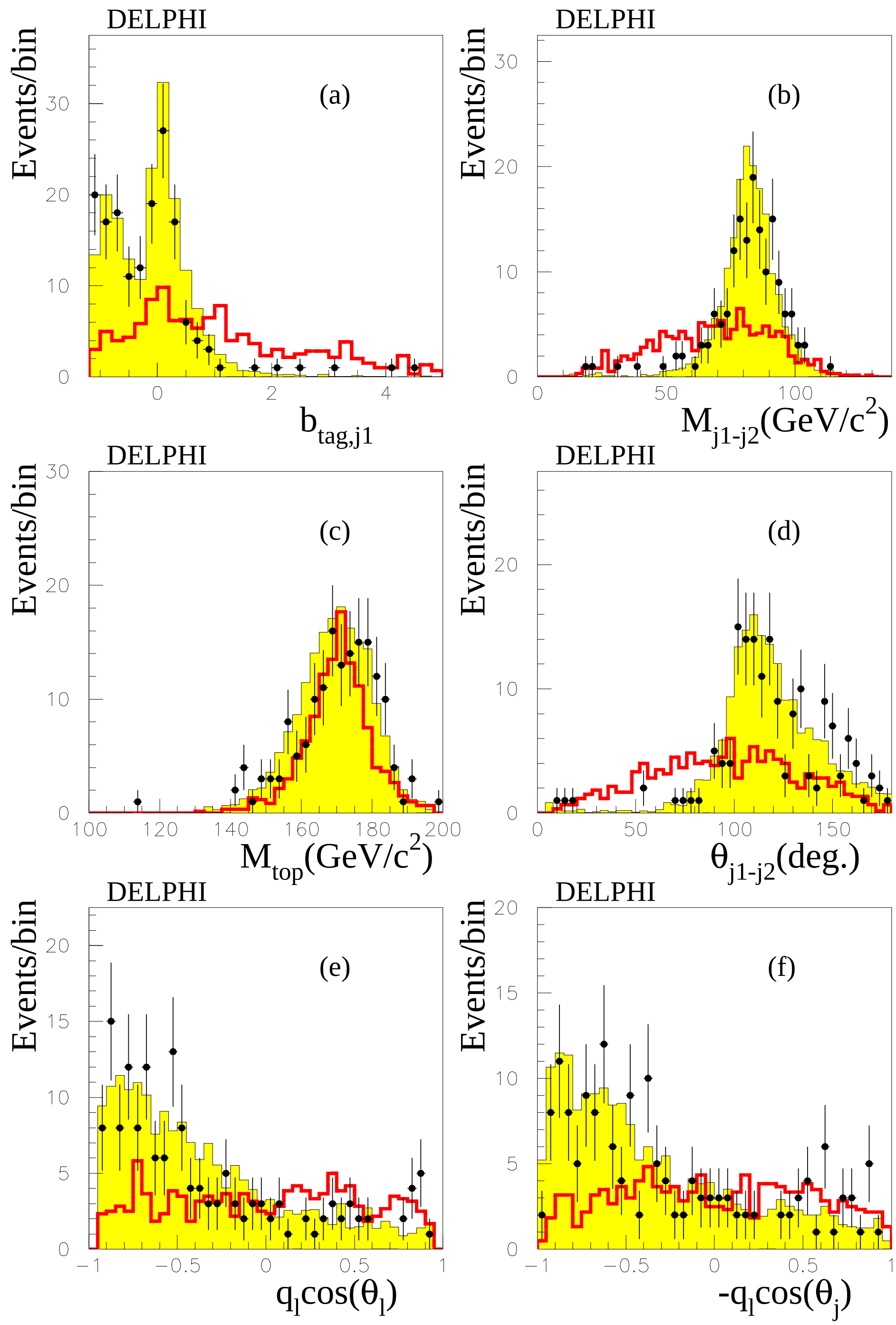

Figure 5: Distributions of relevant variables at the preselection level in the semileptonic decay channel, for $\sqrt{s} = 205 - 207$ GeV: (a) the most energetic jet b-tag parameter, (b) the reconstructed two jet system mass, (c) top mass, (d) the angle between the jets, (e) $\mathrm{q_l}\cos(\theta_\mathrm{l})$ (see text for explanation) and (f) $-\mathrm{q_l}\cos(\theta_\mathrm{j})$. The dots show the data, the shaded region the SM simulation and the thick line the expected signal behaviour (with arbitrary normalization) for a top quark mass of 175 GeV/c^2.

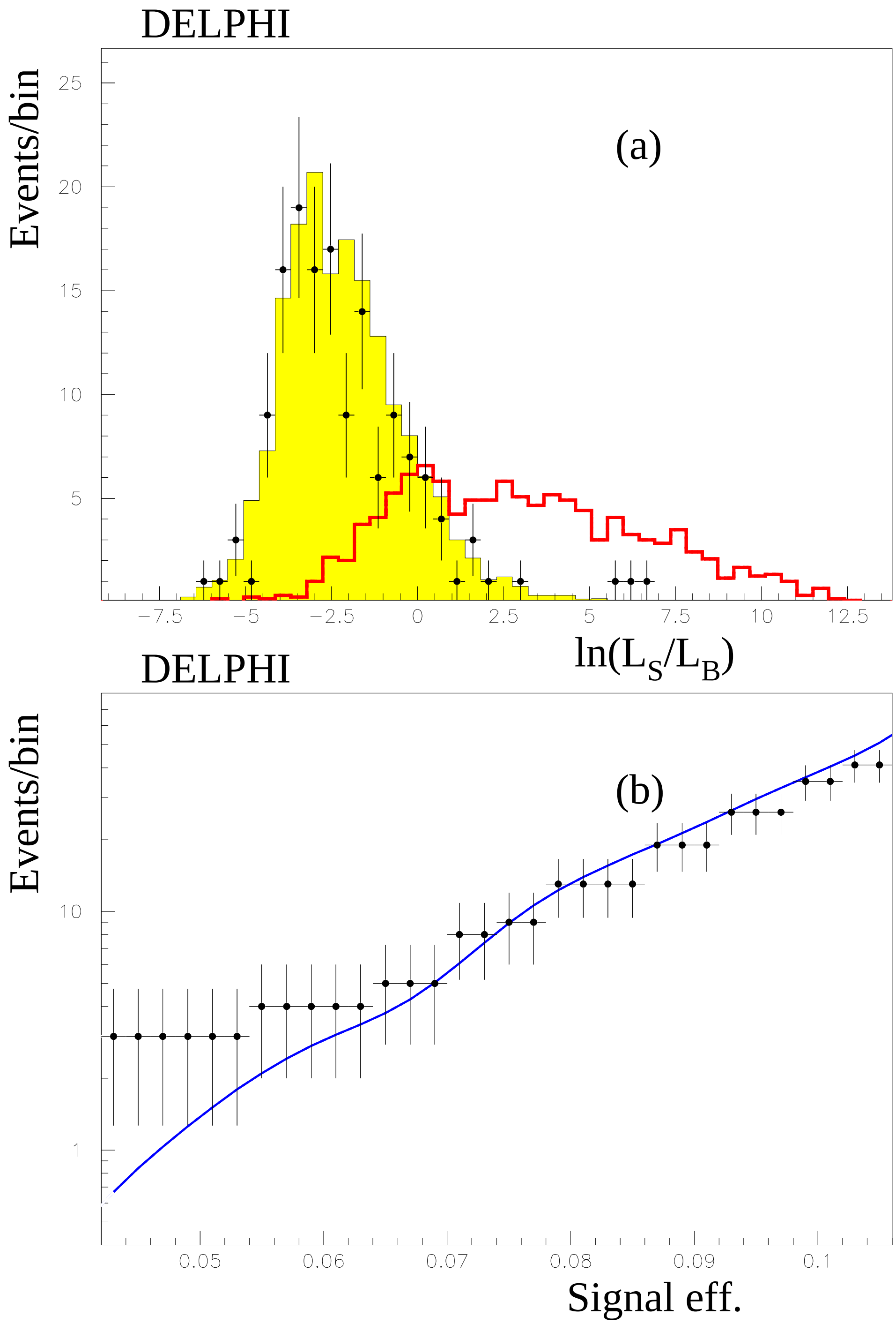

Figure 6: (a) the discriminant variable distribution for $\sqrt{s} = 205-207$ GeV is shown. The dots show the data, the shaded region the SM simulation and the thick line the expected signal behaviour (with arbitrary normalization) for a top quark mass of 175 GeV/c^2. (b) number of accepted data events (dots) together with the expected SM background simulation (full line) as a function of the signal efficiency (convoluted with the W leptonic branching ratio) for a top mass of 175 GeV/c^2.

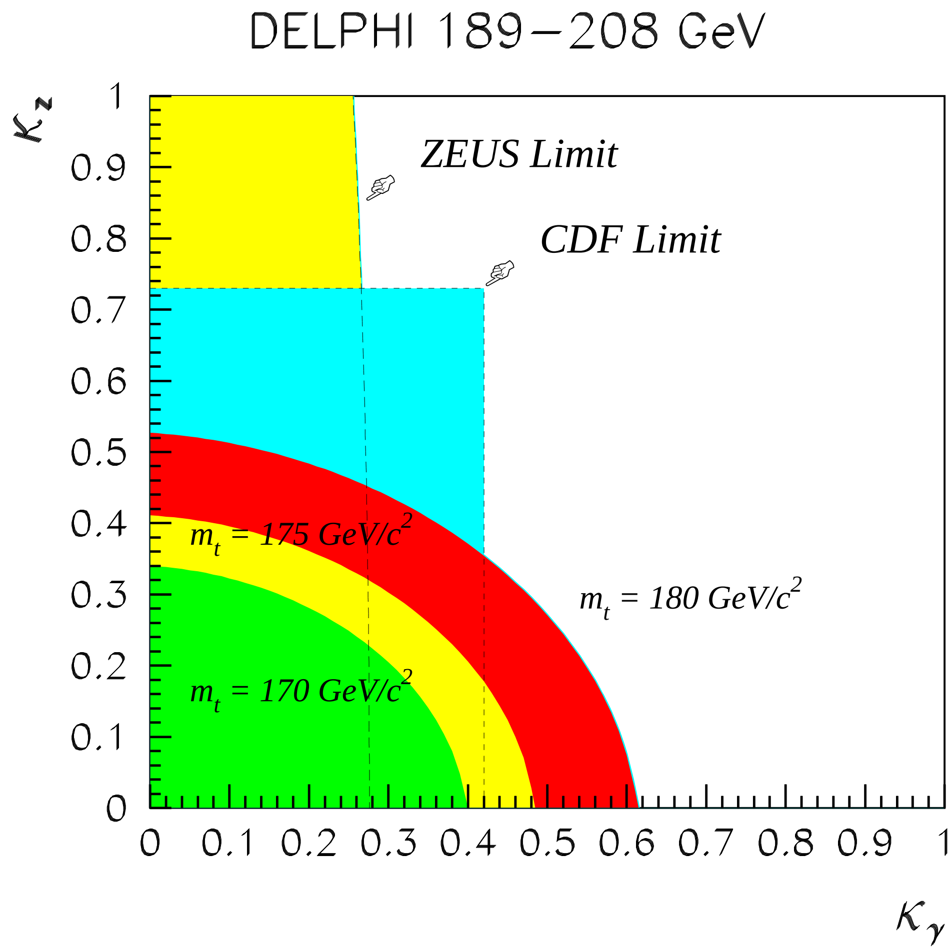

Figure 7: Limits at 95% confidence level in the $\kappa_\gamma - \kappa_Z$ plane. The different curved and filled areas represent the regions allowed by DELPHI for different top quark masses. Radiative corrections were taken into account in the total production cross-section at LEP. The CDF and ZEUS allowed regions are also shown for a top quark mass of 175 GeV/c^2. The ZEUS limits are scaled by a factor of $\sqrt{2}$ because of the difference in the Lagrangian definitions.